Gut Science

Epithelial and stromal remodelling in murine Crohn's disease-like ileitis

Katherine C Letai ,[1,2] Bianca N Islam ,[3,4] Paola Menghini ,[4] Carlo De Salvo ,[5] Neha Khandekar ,[4,6] Bruce Armstrong ,[1,7] Alka Tomar ,[1,2] Kimberly Curry ,[6,8] Theresa T Pizarro ,[5] Paul J Tesar ,[1,2] Marissa A Scavuzzo ,[1,2] Fabio Cominelli [3,4]

To cite: Letai KC, Islam BN, Menghini P, *et al*. Epithelial and stromal remodelling in murine Crohn's disease-like ileitis. *Gut Sci* 2026;**1**:e000008. doi:10.1136/gutsci-2025-000008

► Additional supplemental material is published online only. To view, please visit the journal online (https://doi.org/10.1136/gutsci-2025-000008).

KCL and BNI are joint first authors.
MAS and FC are joint senior authors.

Received 19 November 2025
Accepted 29 December 2025

For numbered affiliations see end of article.

Correspondence to
Dr Fabio Cominelli; fabio.cominelli@uhhospitals.org and
Dr Marissa A Scavuzzo; marissa.scavuzzo@case.edu

ABSTRACT

Background Inflammatory bowel disease is characterised by progressive epithelial, immune and stromal dysfunction. Human datasets yield important insights yet are inherently descriptive, requiring animal models for in vivo mechanistic interrogation. The SAMP1/YitFc (SAMP) mouse model develops spontaneous Crohn's disease (CD)-like ileitis, allowing for the controlled manipulation of pathophysiological pathways.

Objective To define cell-specific disease-associated transcriptional changes and their translational relevance, we profiled inflamed SAMP ilea by single-nucleus RNA-sequencing (snRNA-seq) and compared identified programmes with human IBD single-cell RNA-seq datasets.

Design We performed whole-ileum snRNA-seq on SAMP (n=4) and control AKR/J (n=3) mice using the gut-optimised CitraPrep protocol, generating 58 349 high-quality nuclei across epithelial, immune and stromal lineages. We corroborated SAMP-associated changes with immunofluorescent staining, western blotting, spatial transcriptomic and human single-cell RNA-seq data.

Results We observed a primary type 2 immune phenotype in SAMP compared with AKR mice, but most transcriptional changes occurred in stromal and epithelial, not immune, cells. Stromal remodelling included increased fibroblast-derived *Igf1*. In SAMP epithelium, expansion of tuft cells and emergence of SAMP-specific *Pcsk6+* crypt enterocytes were observed and confirmed in patients with CD. Finally, we identified cross-compartmental changes in cell–cell signalling, including enterocyte-to-type three innate lymphoid cell communication and enhanced global *Igf1* signalling. These features recapitulate both known and novel characteristics of CD, thereby extending our understanding of disease-associated multicellular networks.

Conclusion This atlas of ileitis-prone SAMP mice provides a high-resolution resource for dissecting conserved and novel mechanisms of inflammation and tissue remodelling. In this study, we uncover disease-associated transcriptional changes conserved in human CD, presenting a translational platform for future mechanistic and therapeutic studies.

WHAT IS ALREADY KNOWN ON THIS TOPIC

⇒ Animal models of IBD are essential to discover pathogenic mechanism and test new treatment modalities. The SAMP1Yit/FC mouse model of ileitis is one of the few models that recapitulate the genetic and immunological complexity of the human condition. A complete understanding of how individual cell types in this model reflect human disease is unknown.

WHAT THIS STUDY ADDS

⇒ In this study, we defined disease-associated changes in cellular composition and gene expression of immune, stromal and epithelial cells. While corroborating known key features of SAMP Crohn's disease (CD)-like ileitis, including T helper type 2-immune activation and expansion of Paneth cells, we also revealed novel findings including tuft cell expansion and presence of SAMP-specific PCSK6+ enterocytes, and highlighted a stromal source of insulin-like growth factor 1 in intestinal inflammation. Finally, we show shared transcriptional signatures between our murine data and CD.

HOW THIS STUDY MIGHT AFFECT RESEARCH, PRACTICE OR POLICY

⇒ This work establishes a high-resolution framework for mechanistic exploration and identification of novel therapeutic targets for chronic ileitis.

INTRODUCTION

Inflammatory bowel disease (IBD) comprises a group of chronic, relapsing inflammatory disorders of the gastrointestinal tract, with Crohn's disease (CD) representing one of its more severe and complex forms.[1] While significant strides have been made in understanding IBD pathogenesis, mechanistic insights into cell type-specific alterations remain limited, in part due to the complexity of the human condition and the lack of fully representative animal models.

SAMP1/YitFc (SAMP) mice represent a spontaneous model of CD-like ileitis that shares similar features to disease in patients with CD, including transmural inflammation, mucosal ulceration, lymphoid aggregates

and occasionally, granuloma formation.[2 3] Importantly, SAMP mice exhibit a polygenic, microbially-influenced disease process without the need for chemical induction or genetic engineering, positioning them as a uniquely valuable model for studying the interplay of genetic susceptibility, epithelial barrier dysfunction, immune dysregulation and environmental triggers in IBD. We have previously shown that the primary defect conferring ileitis in SAMP mice originates from a non-haematopoietic source.[4] However, the specific cell type and related transcriptomic profile involved in this process have not been determined.

Recent advances in single-cell and single-nucleus RNA sequencing have enabled unprecedented resolution in profiling tissue heterogeneity, allowing researchers to delineate cell-type-specific transcriptional programmes and infer intercellular interactions.[5] Single-nucleus RNA sequencing (snRNA-seq) offers practical advantages in tissues that are difficult to dissociate or to preserve intact cells without biasing populations, such as full-thickness intestinal tissues, which is further complicated during disease by fibrosis and inflammatory processes. Large human IBD atlases have relied on separate dissociation steps of isolating epithelial and lamina propria fractions, and when whole tissues were processed, fragile cell types were often lost, leaving mainly fibroblasts and muscle. By contrast, the recently developed CitraPrep protocol preserves RNA integrity across all compartments, enabling high-quality profiling of intestinal tissues that was previously unachievable.[6] This represents a major advance over traditional single-cell workflows, where high concentrations of digestive enzymes often degraded RNA and limited approaches to restricted populations of cells. Despite the growing application of these technologies to human IBD, there remains a paucity of single-cell atlases derived from preclinical models of CD-like ileitis. Generating these atlases is critical for aligning model systems with human disease biology and distinguishing conserved from context-specific pathways.

In this study, we perform snRNA-seq and spatial transcriptomics to whole ileal tissues from SAMP mice with established disease and compared their gene signature(s) to healthy control AKR mice, generating a multicompartmental transcriptional atlas of chronic ileitis. We defined disease-associated shifts in cellular composition and gene expression of immune, stromal and epithelial cells. These changes corroborated known key features of SAMP chronic ileitis, including T helper type 2 (Th2) immune activation and expansion of Paneth cells,[7–9] but also revealed novel findings, such as tuft cell expansion and presence of SAMP-specific *Pcsk6*+ enterocytes, and highlighted a stromal source of insulin-like growth factor 1 (IGF1) in intestinal inflammation.

We applied cross-species integration with a large human single-cell RNA-seq dataset[10] and interactome analysis across 26 cell types to define inflammation-driven transcriptional programmes and ligand-receptor network rewiring in chronic ileitis. This high-resolution framework enables mechanistic investigation and therapeutic target discovery and supports the use of spontaneous murine models for preclinical IBD research.

RESULTS

A global single nucleus transcriptional blueprint of ileitis-prone SAMP ilea unveils disease-associated transcriptional changes in every cell type

To investigate disease-associated transcriptional changes at the single-cell level, we collected whole ileal tissues from four 20-week-old SAMP1/YitFc (SAMP) mice with spontaneous ileitis and three healthy AKR (parental) controls. Gross dissection revealed inflamed, thickened ileal tissue in SAMP mice (online supplemental figure 1A). Histological scoring confirmed severe ileal inflammation in SAMP compared with AKR mice (figure 1A). We isolated nuclei using the recently developed gut-optimised CitraPrep method[6] (online supplemental figure 1B), allowing snRNA-seq of these samples (figure 1B). Filtering out low-quality nuclei and doublets produced 58 349 high-quality single-nuclear transcriptomes (online supplemental figure 1C-E).[11–20] Based on unsupervised clustering and marker expression, nuclei were divided into three major tissue compartments: epithelial (81%), immune (10%) and stromal (9%) (figure 1F–G, online supplemental figure 1F, online supplemental table 1), exhibiting well-established cell-specific gene markers (eg, *Vil1, Ptprc, Acta2*, respectively) (figure 1H). This compartmental distribution in mouse ileal tissues approximates the cellular composition reported in human single-cell datasets of healthy ileum, where ~80–90% of cells are epithelial, 8–15% immune and 5–10% stromal, supporting the biological relevance of our murine dataset.[21–23] To ensure statistical robustness, we applied pseudobulk differential expression analysis that aggregates nuclei by biological replicate, a more stringent approach than single-cell-level testing alone. This analysis revealed that in almost every cell type, more genes were downregulated than upregulated in SAMP compared with AKR mice, similar to patterns seen in human ileitis (figure 1I).[10]

Dominant type 2 immune activation in SAMP

Next, we sought to identify differences in the immune environment between these two strains at the single cell level. We resolved the immune subatlas by strain and identified the major lymphoid and myeloid lineages in both AKR and SAMP mice, recovering 3077 immune nuclei from AKR and 2748 from SAMP (figure 2A–B). We defined specific cell subtype identities by unsupervised clustering and marker expression, including B and plasma cells, CD4+ and CD8+ T cells, innate lymphoid cells (ILCs), dendritic cells, macrophages, eosinophils, mast cells and cytotoxic lineages (figure 2A–B; online supplemental figure 2A). We further confirmed cell type assignments by visualising expression of known markers for each identity (online supplemental figure 2B). Functional enrichment analysis of upregulated

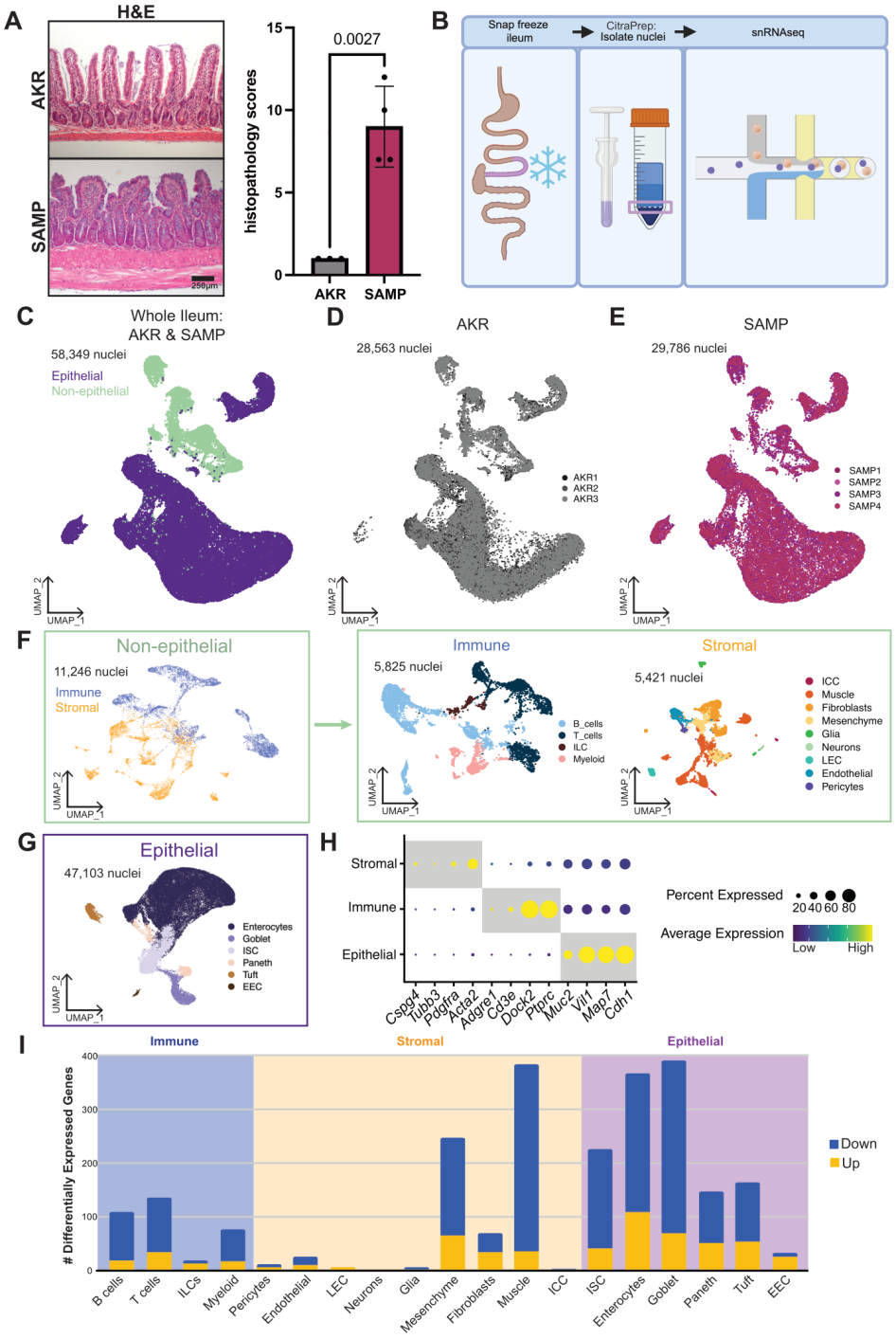

Figure 1 Single nucleus transcriptional blueprint of the murine ileum across epithelial, immune and stromal compartments. (A) Left, representative H&E images illustrate hallmark features of ileitis in SAMP mice, including villous distortion, crypt architectural disruption and prominent leucocytic infiltration in the lamina propria and submucosa. Right, blinded histopathological scoring of ileal inflammation in SAMP versus AKR (n=3–4 per group; exact P shown on plot). (B) Schematic of nuclei isolation and sequencing process. Ileal tissues (10 cm) were harvested from control AKR (n=3) and SAMP (n=4) mice, and nuclei isolated using the CitraPrep protocol for downstream snRNA-seq. (C–E) UMAPs of whole-atlas nuclei from all mice (C), AKR only (D), and SAMP only (E). Nuclei are coloured by cellular compartment in (C) and by biological replicate in (D–E), and visualised with UMAP (n=7 mice, 58 349 nuclei after QC). (F) Non-epithelial cells were split into immune and stromal subatlases, with UMAPs coloured by cell type. (G) Epithelial nuclei are coloured by epithelial cell type and visualised by UMAP. (H) Expression of compartment-specific markers. Dot plot shows canonical markers (rows) across compartments (columns); dot size indicates the fraction of nuclei expressing the gene and colour reflects average scaled expression. (I) Bar graph reporting the number of upregulated and downregulated genes in SAMP versus AKR across major epithelial, immune and stromal lineages (cell type groupings as shown), using thresholds defined in Methods. EEC, enteroendocrine cell; ICC, interstitial Cells of Cajal; ILC, innate lymphoid cell; ISC, intestinal stem cell; LEC, lymphatic endothelial cell; QC, quality control; snRNA-seq, single-nucleus RNA-sequencing; UMAP, Uniform Manifold Approximation and Projection.

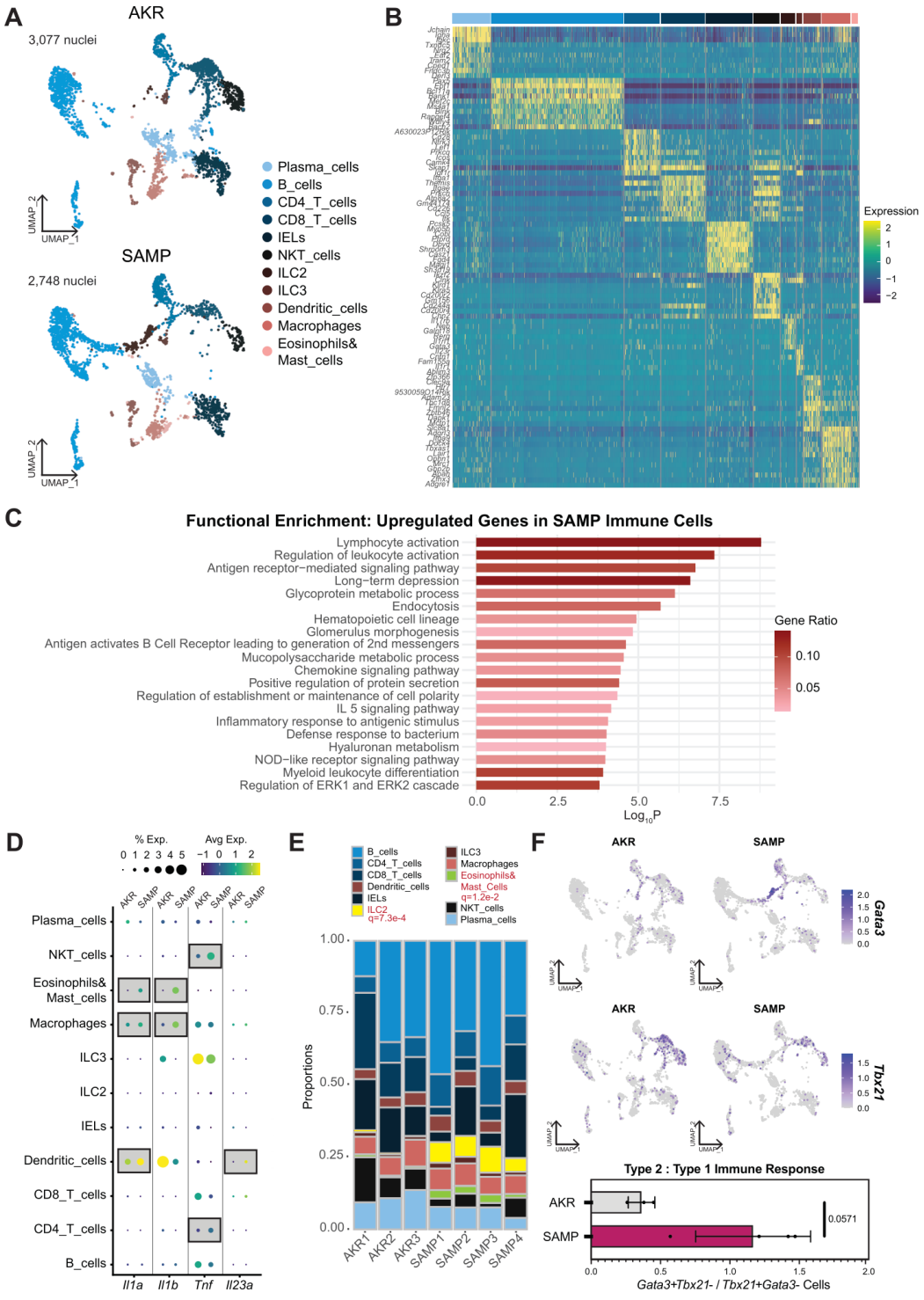

Figure 2 Type 2 immune activation in SAMP ileum. (A) Immune atlas UMAPs stratified by strain, showing AKR (control) and SAMP (disease) nuclei coloured by cell type. Unsupervised clusters are shown in online supplemental figure 2A. (B) Cluster-defining expression heatmap for immune lineages, displaying top 10 transcripts distinguishing each population in rows, and each column representing an individual nucleus, with cell types clustered together and labelled by colour above. Full marker lists are provided in online supplemental table 1. (C) Functional enrichment of genes upregulated in SAMP immune cells, showing Gene Ratio and –log10P as shown for each represented functional term. (D) Dot plot showing *Il1a, Il1b, Tnf* and *Il23a* across immune cell types, stratified by strain. Dot size indicates percent of cells expressing the transcript, and colour indicates relative scaled expression. (E) Per-sample immune cell-type composition (AKR1–3; SAMP1–4), shown as a proportion of the full immune cell population. q values <0.05 are displayed, with labels for expanded populations in red and diminished populations in blue. (F) *Gata3* and *Tbx21* overlaid on strain-specific immune UMAPs, with colour representing normalised expression compared with all genes across all immune cells. Below, quantification of type 2–biased (*Gata3*+*Tbx21*–) versus type 1–biased (*Tbx21*+*Gata3*–) cells (type 2:type 1 ratio shown on plot). IELs, intraepithelial lymphocytes; IL, interleukin; ILC, innate lymphoid cell; NKT, natural killer T cell; UMAP, Uniform Manifold Approximation and Projection.

genes comparing all immune cells in SAMP with those of AKR suggests generalised immune activation and cytokine signalling in SAMP, encompassing a variety of inflammatory response types (figure 2, online supplemental table 2).[24] Furthermore, the CD-associated proinflammatory cytokines, *Il1a, Il1b, Tnf* and *Il23a*, exhibited altered expression patterns across immune cell subpopulations in SAMP versus AKR mice (figure 2D, online supplemental figure 2C), confirming earlier studies.[2] A feature plot of *Ccl21a* and *Ccl19* highlights a statistically significant (adjusted p=0.00059), and a trend towards, decreased expression, respectively, in ilea from SAMP, both of which have been previously shown to be downregulated in SAMP mice (online supplemental figure 2D).[25] Similar to human studies, the immune compartment exhibited fewer transcriptional changes than stromal and epithelial cells (figure 1I).[10] We were therefore particularly interested in assessing changes in cell type proportion between SAMP and AKR immune cells (figure 2).[26] Type 2 immunity orchestrators ILC2s (q=7.3e−4), along with eosinophils and mast cells (q=1.2e−2), were significantly expanded in SAMP, confirming prior studies establishing SAMP mice as a predominant Th2-driven model.[7 8 27] Strain-stratified feature overlays further indicated a shift toward type 2 polarisation in SAMP, reflected by higher *Gata3* relative to *Tbx21* signals and an increased proportion of *Gata3+Tbx21−* versus *Tbx21+Gata3-* cells (figure 2F). Concordantly, the Th2 cytokines, *Il5, Il4* and *Il13*, exhibited higher expression in SAMP immune cells than AKR (online supplemental figure 2C). These analyses defined the immune landscape of the SAMP ileum and detailed a Th2-leaning inflammatory milieu, substantiating previous characterisation of the SAMP mouse and opening the door for subsequent epithelial–immune–stromal interaction studies.

SAMP fibroblasts exhibit profibrotic and proinflammatory transcriptional activation

Beyond immune changes, we also asked whether the stromal compartment differed in gene expression patterns between SAMP and AKR mice. Consolidation of unsupervised clusters of stromal cells based on similar transcriptomic profiles indicated representation of mesenchymal, endothelial and neural lineages in both AKR and SAMP ilea (figure 3A–B, online supplemental figure 3A-B). Given the known disease-related changes in fibroblasts in IBD, we asked whether SAMP fibroblasts transcriptionally shift towards an activated subtype.[28 29] As expected, fibroblasts from SAMP mice displayed significant upregulation of a cohort of transcripts (*Fn1*, *Postn*, *Timp1*, *Ccl2*, *Pdgfra*, *Lox*, *Tnc*, *Wnt2b*, *Il11* and *Cxcl1*) related to inflammation and fibrosis compared with AKR controls (p=9.7e−15, figure 3C), confirming a robust fibrotic phenotype in SAMP ilea.[30 31] A key upregulated gene revealed by differential expression analysis was *Igf1* (figure 3D–E, online supplemental table 2). In patients with CD, *IGF1* has been implicated in intestinal extracellular matrix (ECM) collagen regulation, aggravation of fibrosis and facilitation of malignant transformation.[32 33] To understand whether fibroblasts may be a source of IGF1 protein, we performed multiplexed immunofluorescent staining and confirmed elevated IGF1 in COL1A1+ACTA2+ fibroblasts in SAMP ilea compared with AKR (figure 3F). *Igf1* upregulation is just one of many changes in fibroblast gene expression, so we next asked what other functional changes are implied by these changes. Functional enrichment analysis revealed upregulation of pathways involved in extracellular matrix remodelling, actin filament-based movement and cell migration, while downregulated programmes included interferon signalling and proteoglycan metabolism (figure 3G). Given that muscle cells exhibit the greatest amount of transcriptional change out of stromal cells (figure 1I), as well as the dramatic thickening of the muscle layer observed on histology (figure 1A), we also wanted to understand which transcripts were changing in myocytes of SAMP mice. Notably, we found downregulation of *Calm1* and *Calm3* in SAMP muscle cells, which both code for Calmodulin, a critical protein for proper muscle contraction (online supplemental figure 3C, online supplemental table 2). Functional enrichment analysis (online supplemental figure 3D) indicates mostly metabolic and inflammatory changes, suggestive of adaptive myocytes adapting to an inflammatory environment. Aside from mesenchymal cells, all other stromal cell types, including enteric nervous system cells, exhibited minimal transcriptional differences between SAMP and AKR strains (figure 1A).

Expansion of secretory lineages and emergence of *Pcsk6+* enterocytes in ileitis

We next asked what transcriptional changes occur in the diseased epithelium. Unsupervised clustering of 47 103 epithelial nuclei identified six canonical cell types: enterocytes, goblet cells, intestinal stem cells, Paneth cells, tuft cells and enteroendocrine cells (figure 4A–B; online supplemental figure 4A-B). In our analyses, the proportion of SAMP epithelial cells was biased towards the secretory lineage (q=4.6e−5, online supplemental figure 4C). Specifically, SAMP mice exhibited a significant expansion of Paneth cells, consistent with prior reports[34–36] and newly reported expansion of tuft cells relative to AKR controls (figure 4C), with tuft cell enrichment validated by DCLK1 immunostaining (p=0.0083, figure 4D–E).

To identify the most salient transcriptional changes in the SAMP epithelium, we performed differential expression analysis comparing all epithelial cells across strains (figure 4F–G, online supplemental table 2). Functional enrichment analysis highlighted that SAMP-derived epithelial cells exhibited upregulated markers associated with epithelial inflammation, stress and remodelling, including *Reg4*, *Ang4*, *Cd55* and *Duox2* (figure 4F). One of the top upregulated genes in SAMP was *Pcsk6*, encoding proprotein convertase subtilisin/kexin type 6 (figure 4G). PCSK6 is a calcium-dependent serine protease that cleaves proteins to their active forms

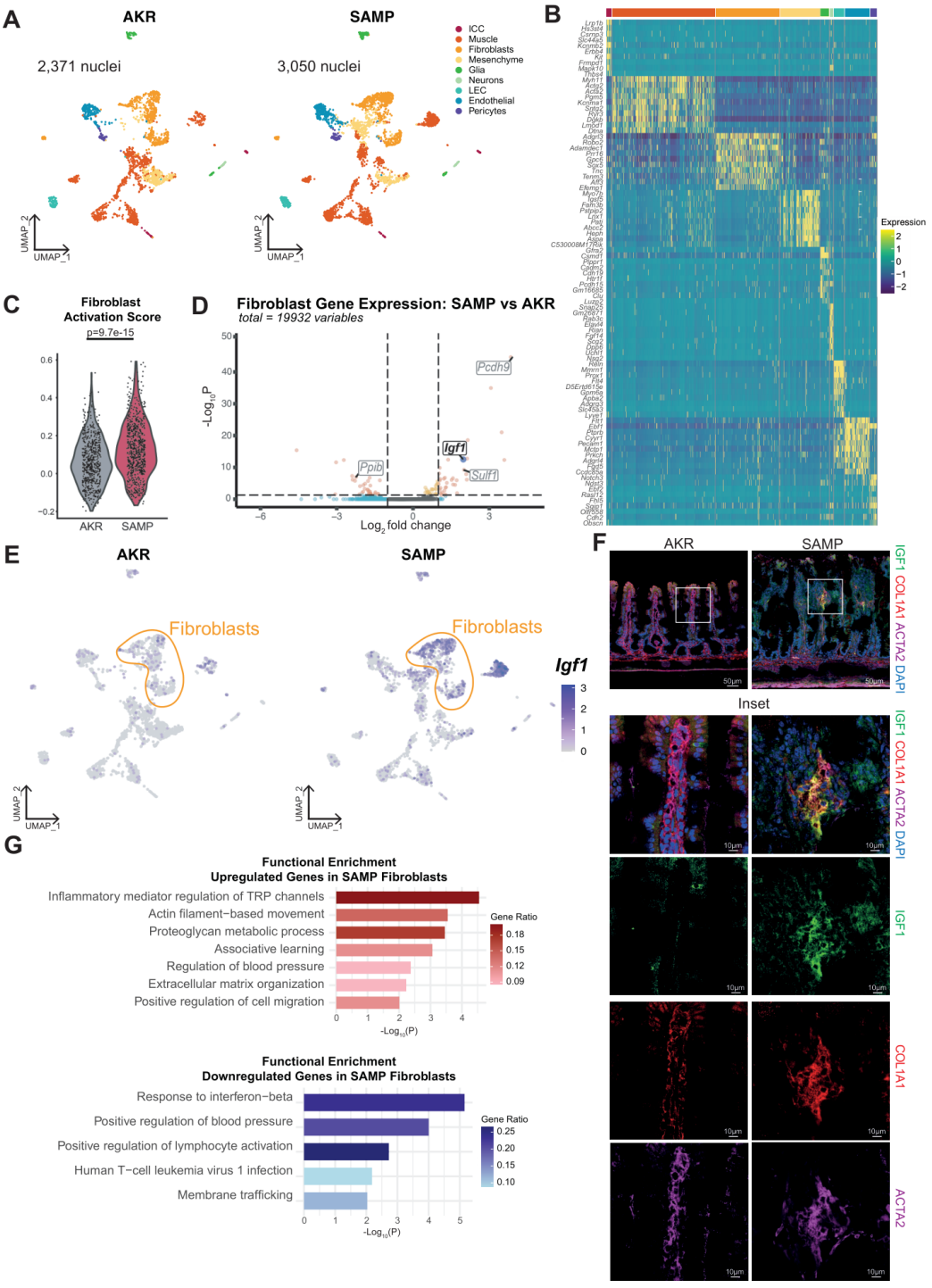

Figure 3 Stromal remodelling in SAMP ilea indicates fibroblast activation and increased IGF1 expression. (A) Stromal nuclei from AKR and SAMP animals plotted separately by UMAP and coloured by cell type to visualise population differences. Unsupervised clusters are shown in online supplemental figure 3A. (B) Top 10 transcripts enriched in each stromal cell type. Individual transcripts are shown in rows, cell types are clustered together in columns with colour annotation above. Full marker lists are provided in online supplemental table 1. (C) Fibroblast Activation Score in AKR and SAMP, p=9.7e−15. Module score was calculated using average expression of the *Fn1*, *Postn*, *Timp1*, *Ccl2*, *Pdgfra*, *Lox*, *Tnc*, *Wnt2b*, *Il11* and *Cxcl1*. (D) Differential gene expression in SAMP fibroblasts compared with AKR visualised as a volcano plot. Log_2 fold change (x-axis) and $-Log_{10}P$ calculated using DESeq2 pseudobulk analysis. (E) *Igf1* expression in AKR and SAMP stroma plotted separately for visualisation in UMAP space. Colour represents normalised expression compared with all genes across all stromal cells. Fibroblasts are circled. (F) Immunofluorescent staining of IGF1 in ACTA2+COL1 A1+ fibroblasts shows an increase in SAMP compared with AKR ileum. (G) Functional enrichment analysis of upregulated and downregulated genes in SAMP fibroblasts. –log10P for each represented functional term is plotted, coloured by gene ratio. ICC, interstitial cells of Cajal; IGF1, insulin-like growth factor 1; LEC, lymphatic endothelial cell; TRP, transient receptor potential; UMAP, Uniform Manifold Approximation and Projection.

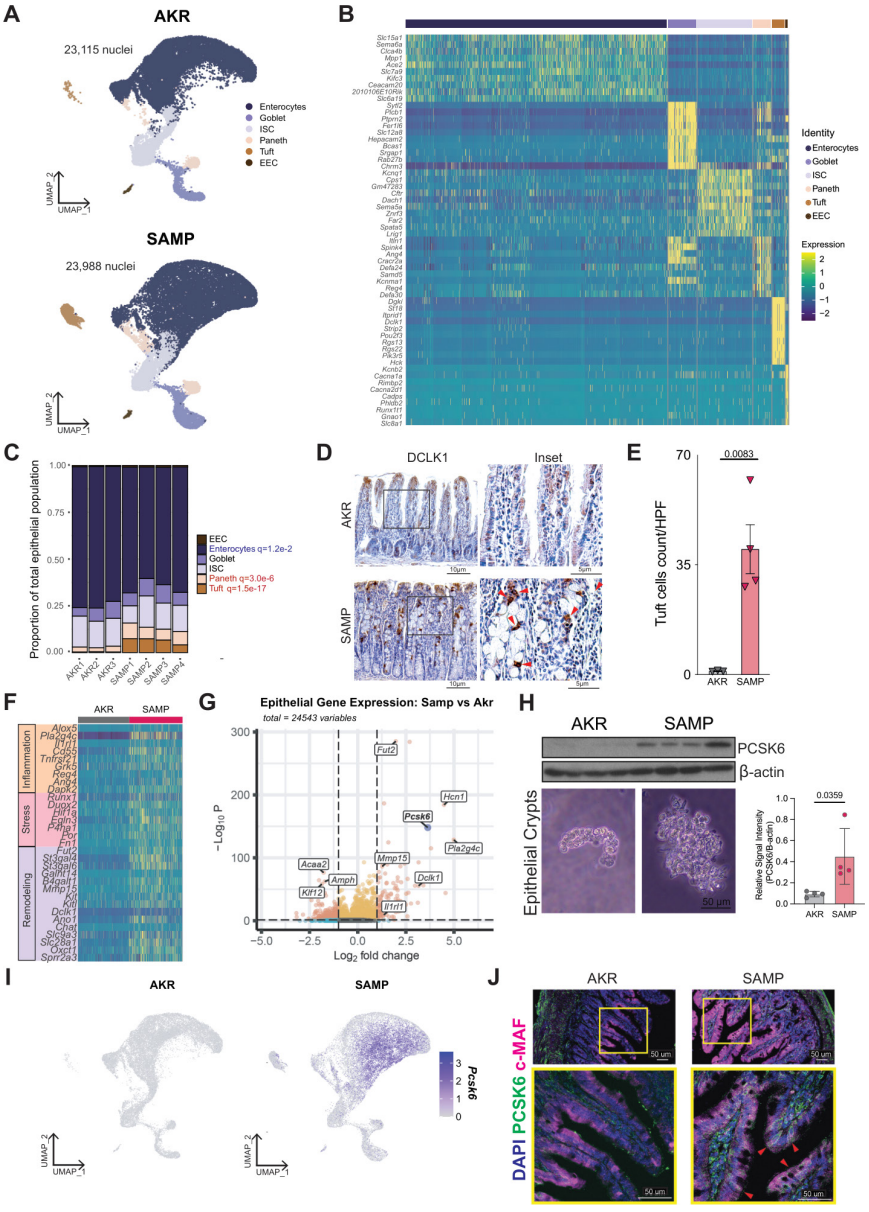

Figure 4 Secretory expansion and PCSK6+ enterocyte in the SAMP epithelial compartment. (A) Epithelial nuclei from AKR and SAMP animals plotted separately and coloured by cell type to visualise population differences. Visualised by UMAP. Unsupervised clusters shown in online supplemental figure 4AD. (B) Top 10 transcripts enriched in each epithelial cell type. Individual transcripts are shown in rows, cell types are clustered together in columns with colour annotation above. Datasets are provided in online supplemental table 1. (C) Fraction of nuclei of each cell type out of all epithelial nuclei per sample. All q values <0.05 listed in red for populations expanded in SAMP, and blue for populations decreased. (D) Immunohistochemistry of the tuft cell marker DCLK1 in both AKR and SAMP tissues, with inset showing example fields used for quantification. Red arrows mark nucleated tuft cells. (E) Quantification of tuft cell numbers normalised per high power field (20×) in AKR and SAMP ilea. Each point represents one animal, with error bars representing SE and p value (0.083) calculated from a two-sample t-test. (F) SAMP tissues exhibit disease-related transcriptional changes. Heatmap of genes involved in inflammation, stress and tissue remodelling. Individual transcripts are shown in rows, organised by category, and cells are clustered by disease status in columns with colour annotation above. (G) Differential gene expression in SAMP epithelial cells compared with AKR visualised as a volcano plot. Log_2 fold change (x-axis) and $-Log_{10}P$ calculated using DESeq2 pseudobulk analysis to retain biological replicate. Select genes of interest annotated, with further investigation focused on *Pcsk6* (bold, purple data point). (H) On the left, Western blot analysis of PCSK6 in isolated ileal crypt-villus units from AKR and SAMP, with representative brightfield images from crypt isolation shown below. Each column represents protein from a different mouse, with ß-actin shown in the second row as a loading control. On the right, quantification of PCSK6 in each mouse normalised by ß-actin. (I) *Pcsk6* expression in AKR and SAMP epithelium plotted separately for visualisation of this DEG in UMAP space. Colour represents normalised expression compared with all genes across all epithelial cells. (J) Immunofluorescent staining of PCSK6 in epithelial crypt-villus from AKR and SAMP ileum, images taken at 20× are shown at the top, with high power images (60×) in the yellow boxed inset for better visualisation. Red arrows mark example PCSK6+enterocytes. DEG, differentially expressed gene; EEC, enteroendocrine cell; HPF, high power field; ISC, intestinal stem cell; UMAP, Uniform Manifold Approximation and Projection.

and was previously shown to promote Th1 differentiation in colitis by activating signal transducer and activator of transcription 1 (STAT1).[37] Western blot of epithelial crypt-villus units[38] confirms the upregulation observed in snRNA-seq is maintained at the protein level (figure 4H), with the potential to have functional effects. We next visualised *Pcsk6* across all epithelial cell subtypes, revealing that expression is primarily restricted to a unique subset of enterocytes only present in SAMP tissues, Enterocyte7 (figure 4I, online supplemental figure 4D-E). Functional enrichment analysis of the top 100 marker genes of this enterocyte cluster suggested changes to metabolic and immune-related programmes (online supplemental figure 4F), including multiple terms related to extracellular matrix production and glycosylation. Immunofluorescent staining of SAMP and AKR tissues confirmed the appearance of PCSK6 protein in a subset of SAMP enterocytes (c-MAF+) (figure 4J), illustrating the specificity of this enterocyte subtype in the diseased ileum. Beyond *Pcsk6,* SAMP enterocytes also upregulated *Il1rl1* (ST2) at both the transcript and protein levels, suggesting interleukin (IL)-33 responsiveness and a further contribution to epithelial–immune signalling (online supplemental figure 4G-H).

Spatial transcriptomics and human single cell validation of the SAMP ileal atlas

To contextualise the potential functional changes of SAMP epithelial cells, we wanted to know whether epithelial programmes identified by snRNA-seq were spatially localised in mouse ilea and conserved in human IBD. Due to the discontinuous, patchy nature of disease in SAMP mice, whole ilea harvested for snRNA-seq contained nuclei from both inflamed (cobblestone-like)[39] and non-inflamed regions that cannot be distinguished from each other using this approach. GeoMx enables us to assess compartment-level transcriptomes in AKR and SAMP mice, segregating SAMP tissue into cobblestone/inflamed versus non-cobblestone/non-inflamed regions (figure 5A, (online supplemental figure 5A). Spatial analysis of the epithelial compartment revealed higher transcript counts in SAMP mice for *Pcsk6, Dclk1, Il1rl1, Pla2g4c, Fut2* and *Mmp15* (figure 5B), mirroring the snRNA-seq data (figure 4G). Cobblestone and non-cobblestone regions exhibited similar trends in expression profiles when compared with AKR, suggesting many of the most relevant transcriptional changes in SAMP ilea occur even in the absence of inflammation. Atlas-derived DEGs were also differentially expressed in the immune and stromal compartments of SAMP and AKR mice, with cobblestone and non-cobblestone regions again showing similar expression patterns (online supplemental figure 5B, online supplemental table 1). Together, these spatial transcriptomic data not only confirm our snRNA-seq findings, but also indicate that many disease-associated transcriptional changes occur globally in the SAMP ileum.

We next asked whether the enterocyte changes we observed in the SAMP model were also present in patients with CD. We assessed expression of the top 50 murine Enterocyte7 gene markers in a single-cell RNA-seq dataset[10] derived from human ileal-specific CD. At the gene level, 72% of Enterocyte7 markers displayed increased expression in enterocytes of non-inflamed or inflamed IBD relative to healthy controls, including *Pcsk6* (figure 5C). *PCSK6* was also upregulated in bulk RNA-seq data from patient with ileal CD biopsies of both non-inflamed and inflamed tissue compared with non-IBD controls (online supplemental figure 5D), though the effect is diluted by non-enterocyte cells included in the biopsy.[40] We next calculated module scores of the Enterocyte7 marker panel in human enterocytes. Enterocyte7 score was elevated in non-inflamed and inflamed human enterocytes at both the single cell (figure 5D) and at the biopsy levels (figure 5E) compared with scores derived from healthy ileum, in line with our finding that alterations in SAMP-distinguishing gene expression occur in both affected and unaffected epithelium. This congruency again supports the translational relevance of the Enterocyte7/*Pcsk6*+enterocyte signature in CD-specific ileitis.

Cross-compartment interactome analysis reveals modified cell–cell communication in chronic ileitis

To assess whether transcriptional remodelling alters intercellular communication, we performed ligand–receptor interactome analysis across 26 cell types.[41] Based on the expression of ligands and receptors, this analysis predicted overall interaction strength between cell types. One of the cell–cell communication relationships predicted to be strongest in SAMP compared with AKR ileum is enterocyte signalling to ILC3s (figure 6A), confirming the importance of this ILC subset in the pathogenesis of SAMP ileitis.[42] Both disease-only and disease-upregulated interactome pairs were identified between enterocytes and ILC3s (figure 6B). Interestingly, examination of ligand expression across enterocyte subclusters revealed that the ILC3-activating signal, *Kitl*, is expressed specifically in the *Pcsk6*+Enterocyte7 cluster (figure 6C), providing additional evidence that this SAMP-restricted enterocyte state may promote tissue inflammation.

To predict which cell types exhibited the most change in cell–cell signalling in SAMP tissues compared with AKR, the tissue-wide interactome analysis summed absolute values in the changes of interaction strengths across all ligand-receptor pairs (figure 6A). Fibroblasts had the greatest amount of predicted change in outgoing signalling, mostly weakening their outgoing interactions in SAMP compared with AKR ileum (figure 6A and D). Examining the strength of predicted fibroblast-derived signalling pathways active in SAMP versus AKR tissues revealed IGF was the only pathway predicted to be active exclusively in SAMP fibroblasts (figure 6D). Visualising IGF signalling across all cells in our dataset demonstrated that IGF signals were initiated only by glia in AKR mice (figure 6E). In contrast, there was extensive rewiring of IGF signalling predicted in SAMP, with fibroblasts as the most prominent source, as well as ILC3s and CD4+ T cells (figure 6E). The interactome predictions indicated that the IGF signal was received by almost every cell type and further suggested IGF was one of the most enriched signalling pathways in SAMP across all cell types (figure 6E). Since

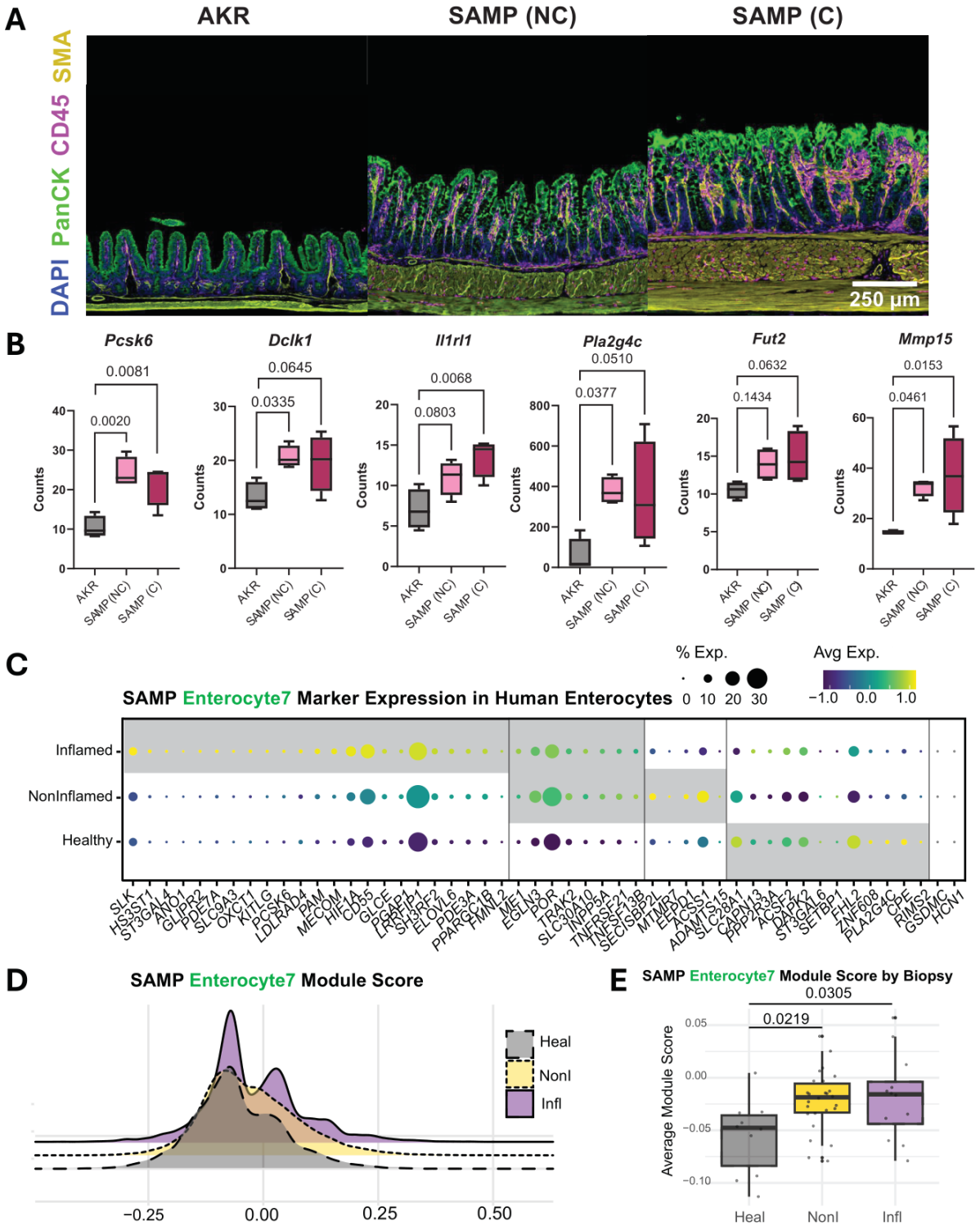

Figure 5 Spatial transcriptomics and human single-cell data validate epithelial programmes from the SAMP ileal atlas. (A) Mouse spatial transcriptomics of ileum comparing AKR and SAMP regions of interest. Representative images showing tissue architecture in AKR and SAMP (both non-cobblestone and cobblestone regions with nuclei (DAPI), epithelium (PanCK), immune infiltrates (CD45), and stromal compartment (SMA) overlays, scale bar 250 um. (B) Box plots of spatial expression for PanCK+ genes across AKR, SAMP NC (non-cobblestone), and SAMP C (cobblestone) regions; exact p values displayed. (C) Dot plot of SAMP Enterocyte7 marker genes in human ileal enterocytes across healthy, non-inflamed IBD and inflamed IBD cohorts; dot size denotes percent expressing and colour indicates average scaled expression. Grey boxes highlight (left-to-right) transcripts elevated primarily in inflamed tissue, similarly elevated in inflamed and non-inflamed, elevated in non-inflamed only, and similar or elevated in healthy cells. (D) Ridge plot of Enterocyte7 module score distribution across human enterocytes for healthy, non-inflamed and inflamed groups. (E) Per-sample Enterocyte7 module scores in the human dataset, displaying individual patients with group medians/IQRs; exact p values reported on panel. C, cobblestone; Heal, healthy; Infl, inflamed; NC, non-cobblestone; NonI, non-inflamed.

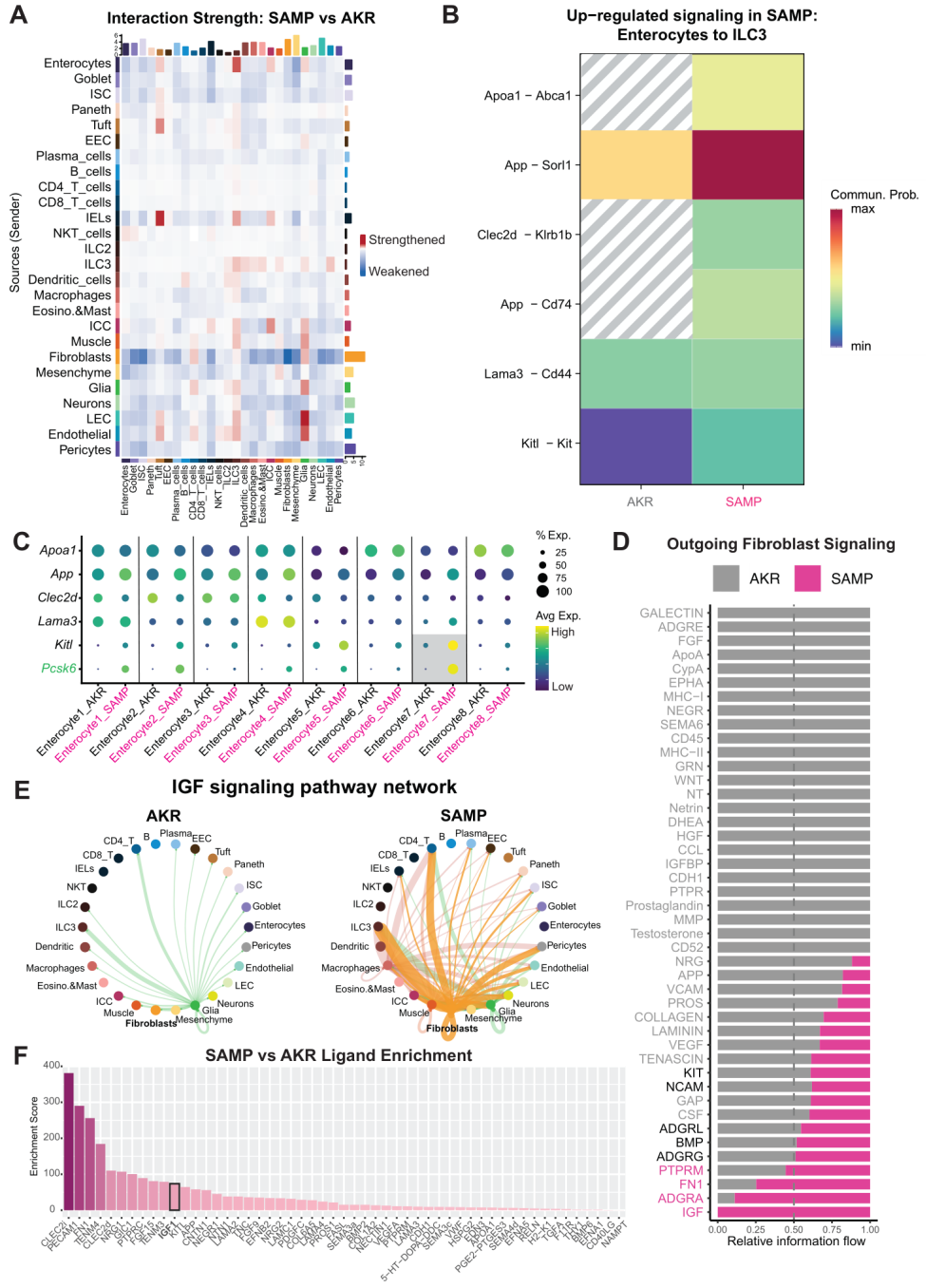

Figure 6 Cross-compartment interactions in SAMP ileum reveal tissue-wide rewiring of inflammation and repair programmes. (A) Heatmap showing the strength of interactions between all cell types in SAMP versus AKR animals, predicted by CellChat. Source cells are plotted on the y-axis, and receiving cells are on the x-axis. Height of bars represents the sum of the absolute values of the heatmap values in that row (righthand bars) or column (top bars) (higher bar means more change for that cell type). (B) Communication probabilities for changed interactions from enterocytes to ILC3s. Probabilities in AKR are listed on the left, and SAMP on the right. Colour represents probability, with red as high and blue low. All interaction probabilities have p values <0.01 when compared between SAMP versus AKR. Grey lines indicate no signalling predicted for that ligand-receptor pair and strain. (C) DotPlot showing expression of the predicted ILC3-sensed ligands transcribed by enterocytes (rows), in SAMP versus AKR cells across all eight enterocyte subtypes in our dataset (columns). *Kitl* exhibits the most dramatic increase in SAMP versus AKR, particularly in Enterocyte7, alongside *Pcsk6* (green). (D) Relative information flow of the fibroblast outgoing signalling network. Information flow is defined as the sum of communication probability among all pairs of cell groups, plotted here by condition as a proportion of the total communication across both conditions (AKR+SAMP). Pathways in grey are enriched in AKR, and those in pink are enriched in SAMP. (E) Circos plots showing IGF signalling in AKR versus SAMP. Lines are coloured like the cell type sending the signal, connecting to cell types predicted to receive the signal, with outgoing fibroblast signals highlighted in purple. (F) Enrichment score for all ligands enriched in SAMP (across all cell types), including IGF (black box). EEC, enteroendocrine cell; ICC, interstitial cells of Cajal; IELs, intraepithelial lymphocytes; IGF, insulin-like growth factor; ILC, innate lymphoid cell; ISC, intestinal stem cell; LEC, lymphatic endothelial cell; NKT, natural killer T cell.

we observed putative rewiring of IGF in the SAMP tissue across many cell types, we next set out to determine broad ligand changes in the inflamed gut. Tissue-wide analysis of ligand transcription predicted SAMP enrichment of not only IGF1 secretion, but also CLEC2i, PECAM1 and others, emphasising that enterocyte-to-ILC3 and IGF signalling are only two of many likely cell–cell signalling changes in SAMP compared with AKR (figure 6F). These putative cross-compartmental interactions indicate that epithelial, immune and stromal cells all actively modulate their microenvironment during chronic disease. This highlights the need for robust experimental animal models to dissect the cellular and molecular choreography in IBD pathogenesis.

DISCUSSION

Using snRNA-seq of whole ileal tissues from SAMP mice with spontaneous chronic ileitis, we delineated compartment-wide transcriptional remodelling spanning epithelial, immune and stromal cell lineages. Our data provide molecular, cell-specific evidence for prior observations of the SAMP pathology, extend the understanding of disease-associated cell states and uncover novel transcriptional programmes that may be relevant to the pathogenesis of CD.

Although CD is classically regarded as an immune-mediated disorder, our results reveal that the most profound transcriptional changes in the SAMP model occur in the epithelial and stromal compartments. This was initially unexpected, given the known importance of T cell-driven inflammation in this model.[2 7] However, this finding aligns with prior work demonstrating that early epithelial alterations occur in SAMP mice, prior to the onset of ileitis, and that epithelial-derived IL-33 promotes early ILC2 expansion in a nucleotide-binding oligomerisation domain-containing protein 2 (NOD2)-dependent and microbiota-dependent manner during the development of ileitis.[4 8] Our current data extend these findings by showing the presence of specific enterocyte subtypes in SAMP mice. In addition, we show upregulation of ST2+ enterocytes and a larger ILC2 population compared with controls. Fibroblasts from SAMP mice exhibited robust activation signatures, including upregulation of *Igf1*, consistent with a phenotype that promotes both fibrosis and epithelial repair. These findings were validated at the protein level by multiplex immunofluorescence. Gene enrichment analysis suggested that fibroblasts in chronic ileitis adopt a pro-repair and migratory state, activating pathways implicated in ECM reorganisation and growth factor signalling. These stromal dynamics provide a unique opportunity to interrogate fibroblast subsets as potential therapeutic targets in chronic intestinal inflammation and IBD-associated fibrosis.

In this study, we observed significant expansion of both Paneth and tuft cells in the SAMP ileum. While increased Paneth cells are consistent with previous reports in this model,[34] tuft cell expansion diverges from human IBD, where tuft cells are typically depleted in inflamed tissue.[10 35 43 44] This distinction may reflect species-specific responses to chronic inflammation or distinct temporal phases of epithelial remodelling. Humans are rarely biopsied until they present with symptoms, raising the possibility that tuft cell expansion represents an early epithelial response captured in this experimental model, but missed in human disease. Both temporal and species-specific explanations, therefore, remain plausible. In parallel, we identified a transcriptionally distinct population of *Pcsk6*+ enterocytes, enriched in the villus-crypt regions of SAMP mice. These cells expressed genes involved in secretory stress, antimicrobial defence and wound healing, suggesting an inflamed crypt-adapted state. Importantly, recent work has shown that PCSK6 promotes colitis progression by binding to and activating STAT1, thereby enhancing Th1 differentiation and M1 macrophage polarisation, while compromising tight junction integrity and barrier function in vivo.[37] In murine models of dextran sodium sulfate (DSS)-induced colitis, PCSK6 deficiency attenuated inflammation, improved epithelial barrier integrity and reduced proinflammatory immune polarisation. The increased expression of *Pcsk6* in inflamed villus-crypts in our model indicates a broader role for epithelial-derived PCSK6 in shaping mucosal immunity and amplifying local inflammation. Together, these data position PCSK6 as an important candidate mediator of epithelial–immune crosstalk in chronic ileitis and support further functional interrogation in vivo.

Spatial transcriptomic mapping confirmed that increased *Pcsk6* was present in both inflamed and non-inflamed SAMP tissue, suggesting a transcriptional change that may precede lesion formation. Notably, parallel analysis of human ileal CD revealed conserved upregulation of the murine Enterocyte7 marker panel, underscoring their translational relevance and establishing SAMP as a preclinical platform for the discovery of human-relevant novel therapeutic targets.

While this study provides a comprehensive snRNA-seq atlas of chronic ileitis in the SAMP model, several technical considerations warrant discussion. First, the use of snRNA-seq, while optimised for frozen tissue, has limitations in capturing predominantly cytoplasmic transcripts. This may be a strength when assessing context-specific changes, in that nuclei sequencing captures nascent transcripts, representing active transcription, rather than long-lived cytoplasmic messenger RNAs. However, inflammatory mediators, such as cytokines, are often under-represented in nuclear transcriptomes, which may obscure certain facets of immune activation.[45] However, key inflammatory programmes were supported by gene module scoring, pathway enrichment and independent protein validation. Second, we observed limited representation of granulocytes, a known limitation of snRNA-seq, due to their particularly fragile nuclei. As such, granulocyte dynamics are likely underestimated and should be further explored using complementary approaches. Despite these caveats, our dataset includes 58 349 high-quality nuclei from whole ileum tissue across

seven animals (n=4 SAMP, n=3 AKR), yielding high statistical power for differential gene expression, cell-type classification and cross-compartment interactome analyses.

The identification of disease-associated transcriptional programmes across epithelial, immune and stromal compartments in the SAMP model offers a foundation for translational research aimed at disrupting chronic intestinal inflammation. Our interactome analysis uncovered expanded ligand–receptor signalling from epithelial and fibroblast compartments involving growth factors (*Igf1, Vegfa, Bmp2*), laminins (*Lama3, Lama4*), and adhesion molecules (*Kitl, App*), many of which are implicated in tissue remodelling, angiogenesis and immune cell recruitment. Several of these pathways are already targeted in cancer or fibrosis therapeutics and may represent underexplored opportunities in IBD.[46–49] For example, fibroblast-derived IGF1 has been shown to regulate epithelial repair and stromal-immune crosstalk,[50] and our protein validation confirms its spatial localisation to fibroblasts during ileitis. The widespread induction of IGF1 signalling across many cell types in the SAMP ileum may also suggest a compelling therapeutic target, with the ability to impact not just one, but several populations in the chronic ileitis microenvironment.

These insights suggest that the SAMP single-nucleus atlas can serve not only as a mechanistic resource but also as a preclinical platform to nominate and functionally test therapeutic candidates that operate across mucosal compartments. Interventions that target both effector T cells and epithelial/stromal drivers may be especially effective in disrupting the self-sustaining loop of inflammation and maladaptive repair characteristic of CD. Spatial and cross-species validation supports these pathways as conserved drivers of mucosal injury and repair, rather than model-specific features. Integrating spatial and human IBD data into the SAMP framework enhances its translational value and prioritises clinically relevant targets.

In summary, this study defines the multicellular architecture of chronic ileitis in SAMP mice, reveals novel disease-associated transcriptional programmes and lays the groundwork for targeted investigations of mucosal inflammation and repair. The inclusion of all major compartments in a single atlas enhances its utility as a reference for future mechanistic and therapeutic studies, particularly in dissecting epithelial–immune–stromal circuits relevant to CD. The identification of *Pcsk6*+ enterocytes, given their known proinflammatory role in colitis, provides an entry point for studying epithelial drivers of immune polarisation and mucosal injury.

Author affiliations
[1]Institute for Glial Sciences, Case Western Reserve University School of Medicine, Cleveland, Ohio, USA
[2]Genetics and Genomic Sciences, Case Western Reserve University School of Medicine, Cleveland, Ohio, USA
[3]Medicine/Gastroenterology and Liver Disease, Case Western Reserve University School of Medicine, Cleveland, Ohio, USA
[4]Digestive Health Research Institute; Division of Gastroenterology and Liver Diseases, Case Western Reserve University, Cleveland, Ohio, USA
[5]Pathology, Case Western Reserve University School of Medicine, Cleveland, Ohio, USA
[6]Case Western Reserve University, Cleveland, Ohio, USA
[7]NEOMED, Rootstown, Ohio, USA
[8]Surgery, Case Western Reserve University, Cleveland, Ohio, USA

Acknowledgements We would like to thank the CWRU Genomics Core for sequencing the libraries generated during this study, and the Cleveland Digestive Disease Research Core Center (DDRCC)'s Histology/Imaging and Mouse Models Cores for histology/IHC services and provision of SAMP/AKR mouse strains, respectively. We would also like to acknowledge Daniele Corridoni and Greet De Baets for their helpful discussion of the human dataset. Many thanks to Katreya Lovrenert for uploading our data to GEO. Finally, we would like to thank the entirety of the Institute for Glial Sciences and the Cleveland DDRCC for productive discussion of this project.

Contributors Conception and design: KCL, BNI, PM, MS, PJT, FC. Data acquisition: KCL, MS, BNI, CDS, PM, BA, NK, AT, KC. Single-cell/nucleus data analysis: KCL. GeoM analysis: BNI, NK. Other data analysis and interpretation: KCL, BNI, CDS. Manuscript preparation: BNI, KCL. Critical revision of the manuscript: MS, FC, PJT, TTP. Study supervision: MS, FC, PJT, TTP. Fabio Cominelli is the guarantor. Funding: PJT, FC, MS, BI.

Funding Cleveland DDRCC Pilot & Feasibility Award, National Institutes of Health R35 NS116842, National Institutes of Health R01 CA160356, National Institutes of Health R01 DK042191, National Institutes of Health T32 GM007250, National Institutes of Health T32 GM152319, National Institutes of Health T32 DK083251, National Institutes of Health P30 DK097948, Howard Hughes Medical Institute Hanna H. Gray Fellowship, Burroughs Wellcome Fund (Postdoctoral Enrichment Program).

Competing interests None declared.

Patient and public involvement Patients and/or the public were not involved in the design, or conduct, or reporting, or dissemination plans of this research.

Patient consent for publication Not applicable.

Ethics approval Not applicable.

Provenance and peer review Not commissioned; externally peer reviewed.

Data availability statement Data are available in a public, open access repository. Data are available upon reasonable request.

ORCID iDs
Katherine C Letai https://orcid.org/0000-0002-5516-3910
Bianca N Islam https://orcid.org/0000-0002-2124-1028
Paola Menghini https://orcid.org/0000-0002-8779-088X
Carlo De Salvo https://orcid.org/0000-0002-1523-1915
Neha Khandekar https://orcid.org/0009-0004-9244-5070
Bruce Armstrong https://orcid.org/0009-0001-5276-493X
Alka Tomar https://orcid.org/0009-0002-7813-2268
Kimberly Curry https://orcid.org/0009-0006-8703-620X
Theresa T Pizarro https://orcid.org/0000-0003-3163-915X
Paul J Tesar https://orcid.org/0000-0003-1532-3155
Marissa A Scavuzzo https://orcid.org/0000-0003-0651-6369
Fabio Cominelli https://orcid.org/0000-0002-1571-1548

REFERENCES

1 Roda G, Chien Ng S, Kotze PG, *et al*. Crohn's disease. *Nat Rev Dis Primers* 2020;6:22.
2 Kosiewicz MM, Nast CC, Krishnan A, *et al*. Th1-type responses mediate spontaneous ileitis in a novel murine model of Crohn's disease. *J Clin Invest* 2001;107:695–702.
3 Pizarro TT, Pastorelli L, Bamias G, *et al*. SAMP1/YitFc mouse strain: a spontaneous model of Crohn's disease-like ileitis. *Inflamm Bowel Dis* 2011;17:2566–84.
4 Olson TS, Reuter BK, Scott KG-E, *et al*. The primary defect in experimental ileitis originates from a nonhematopoietic source. *J Exp Med* 2006;203:541–52.
5 Cuevas-Diaz Duran R, González-Orozco JC, Velasco I, *et al*. Single-cell and single-nuclei RNA sequencing as powerful tools to decipher cellular heterogeneity and dysregulation in neurodegenerative diseases. *Front Cell Dev Biol* 2022;10:884748.
6 Scavuzzo MA, Letai KC, Maeno-Hikichi Y, *et al*. Enteric glial hub cells coordinate intestinal motility. *bioRxiv* 2023.:2023.06.07.544052.
7 Bamias G, Martin C, Mishina M, *et al*. Proinflammatory effects of TH2 cytokines in a murine model of chronic small intestinal inflammation. *Gastroenterology* 2005;128:654–66.
8 De Salvo C, Buela K-A, Creyns B, *et al*. NOD2 drives early IL-33-dependent expansion of group 2 innate lymphoid cells during Crohn's disease-like ileitis. *J Clin Invest* 2021;131:140624.
9 Barnes SL, Vidrich A, Wang M-L, *et al*. Resistin-like molecule beta (RELMbeta/FIZZ2) is highly expressed in the ileum of SAMP1/YitFc mice and is associated with initiation of ileitis. *J Immunol* 2007;179:7012–20.
10 Kong L, Pokatayev V, Lefkovith A, *et al*. The landscape of immune dysregulation in Crohn's disease revealed through single-cell transcriptomic profiling in the ileum and colon. *Immunity* 2023;56:444–58.
11 Korsunsky I, Millard N, Fan J, *et al*. Fast, sensitive and accurate integration of single-cell data with Harmony. *Nat Methods* 2019;16:1289–96.
12 Stuart T, Butler A, Hoffman P, *et al*. Comprehensive Integration of Single-Cell Data. *Cell* 2019;177:1888–902.
13 Satija R, Farrell JA, Gennert D, *et al*. Spatial reconstruction of single-cell gene expression data. *Nat Biotechnol* 2015;33:495–502.
14 Hao Y, Stuart T, Kowalski MH, *et al*. Dictionary learning for integrative, multimodal and scalable single-cell analysis. *Nat Biotechnol* 2024;42:293–304.
15 Hao Y, Hao S, Andersen-Nissen E, *et al*. Integrated analysis of multimodal single-cell data. *Cell* 2021;184:3573–87.
16 Butler A, Hoffman P, Smibert P, *et al*. Integrating single-cell transcriptomic data across different conditions, technologies, and species. *Nat Biotechnol* 2018;36:411–20.
17 Xi NM, Li JJ. Benchmarking Computational Doublet-Detection Methods for Single-Cell RNA Sequencing Data. *Cell Syst* 2021;12:176–94.
18 McGinnis CS, Murrow LM, Gartner ZJ. DoubletFinder: Doublet Detection in Single-Cell RNA Sequencing Data Using Artificial Nearest Neighbors. *Cell Syst* 2019;8:329–37.
19 Drokhlyansky E, Smillie CS, Van Wittenberghe N, *et al*. The Human and Mouse Enteric Nervous System at Single-Cell Resolution. *Cell* 2020;182:1606–22.
20 Fleming SJ, Chaffin MD, Arduini A, *et al*. Unsupervised removal of systematic background noise from droplet-based single-cell experiments using CellBender. *Nat Methods* 2023;20:1323–35.
21 Triana S, Stanifer ML, Metz-Zumaran C, *et al*. Single-cell transcriptomics reveals immune response of intestinal cell types to viral infection. *Mol Syst Biol* 2021;17:e9833.
22 Tang W, Zhong Y, Wei Y, *et al*. Ileum tissue single-cell mRNA sequencing elucidates the cellular architecture of pathophysiological changes associated with weaning in piglets. *BMC Biol* 2022;20:123.
23 Hickey JW, Becker WR, Nevins SA, *et al*. Organization of the human intestine at single-cell resolution. *Nature New Biol* 2023;619:572–84.
24 Zhou Y, Zhou B, Pache L, *et al*. Metascape provides a biologist-oriented resource for the analysis of systems-level datasets. *Nat Commun* 2019;10:1523.
25 Mikulski Z, Johnson R, Shaked I, *et al*. SAMP1/YitFc mice develop ileitis via loss of CCL21 and defects in dendritic cell migration. *Gastroenterology* 2015;148:783–93.
26 Phipson B, Sim CB, Porrello ER, *et al*. propeller: testing for differences in cell type proportions in single cell data. *Bioinformatics* 2022;38:4720–6.
27 De Salvo C, Wang X-M, Pastorelli L, *et al*. IL-33 Drives Eosinophil Infiltration and Pathogenic Type 2 Helper T-Cell Immune Responses Leading to Chronic Experimental Ileitis. *Am J Pathol* 2016;186:885–98.
28 Kinchen J, Chen HH, Parikh K, *et al*. Structural Remodeling of the Human Colonic Mesenchyme in Inflammatory Bowel Disease. *Cell* 2018;175:372–86.
29 Cheng X, Shao P, Wang X, *et al*. Myeloid-Derived Suppressor Cell Accumulation Drives Intestinal Fibrosis through mCCL6/hCCL15 Chemokine-Mediated Fibroblast Activation. *Adv Sci (Weinh)* 2025;12:e2411711.
30 Artone S, Ray S, Williams JJ, *et al*. The angiotensin receptor blocker, losartan, reduces inflammation and fibrosis, and prevents relapse of fibrosis after steroid-induced remission, in mice prone to Crohn's disease-like ileitis. *J Crohns Colitis* 2025;19:jjaf083.
31 Bauer-Rowe KE, Pham B, Griffin M, *et al*. Creeping fat-derived mechanosensitive fibroblasts drive intestinal fibrosis in Crohn's disease strictures. *Cell* 2025;188:6536–53.
32 Zatorski H, Marynowski M, Fichna J. Is insulin-like growth factor 1 (IGF-1) system an attractive target inflammatory bowel diseases? Benefits and limitation of potential therapy. *Pharmacol Rep* 2016;68:809–15.
33 Lawrance IC, Maxwell L, Doe W. Inflammation location, but not type, determines the increase in TGF-beta1 and IGF-1 expression and collagen deposition in IBD intestine. *Inflamm Bowel Dis* 2001;7:16–26.
34 Vidrich A, Buzan JM, Barnes S, *et al*. Altered epithelial cell lineage allocation and global expansion of the crypt epithelial stem cell population are associated with ileitis in SAMP1/YitFc mice. *Am J Pathol* 2005;166:1055–67.
35 Shanahan MT, Vidrich A, Shirafuji Y, *et al*. Elevated Expression of Paneth Cell CRS4C in Ileitis-prone SAMP1/YitFc Mice. *Journal of Biological Chemistry* 2010;285:7493–504.
36 Shimizu Y, Nakamura K, Yoshii A, *et al*. Paneth cell α-defensin misfolding correlates with dysbiosis and ileitis in Crohn's disease model mice. *Life Sci Alliance* 2020;3:e201900592.
37 Mei X, Zhou H, Song Z, *et al*. PCSK6 mediates Th1 differentiation and promotes chronic colitis progression and mucosal barrier injury via STAT1. *Aging (Milano)* 2023;15:4363–73.
38 Nik AM, Carlsson P. Separation of intact intestinal epithelium from mesenchyme. *Biotechniques* 2013;55:42–4.
39 Rodriguez-Palacios A, Kodani T, Kaydo L, *et al*. Stereomicroscopic 3D-pattern profiling of murine and human intestinal inflammation reveals unique structural phenotypes. *Nat Commun* 2015;6:7577.
40 Argmann C, Hou R, Ungaro RC, *et al*. Biopsy and blood-based molecular biomarker of inflammation in IBD. *Gut* 2023;72:1271–87.
41 Jin S, Plikus MV, Nie Q. CellChat for systematic analysis of cell-cell communication from single-cell transcriptomics. *Nat Protoc* 2025;20:180–219.
42 Li Z, Buttó LF, Buela K-A, *et al*. Death Receptor 3 Signaling Controls the Balance between Regulatory and Effector Lymphocytes in SAMP1/YitFc Mice with Crohn's Disease-Like Ileitis. *Front Immunol* 2018;9:362.
43 Kjærgaard S, Jensen TSR, Feddersen UR, *et al*. Decreased number of colonic tuft cells in quiescent ulcerative colitis patients. *Eur J Gastroenterol Hepatol* 2021;33:817–24.
44 Banerjee A, Herring CA, Chen B, *et al*. Succinate Produced by Intestinal Microbes Promotes Specification of Tuft Cells to Suppress Ileal Inflammation. *Gastroenterology* 2020;159:2101–15.
45 Thrupp N, Sala Frigerio C, Wolfs L, *et al*. Single-Nucleus RNA-Seq Is Not Suitable for Detection of Microglial Activation Genes in Humans. *Cell Rep* 2020;32:108189.
46 Janssen J, Varewijck AJ. IGF-IR Targeted Therapy: Past, Present and Future. *Front Endocrinol (Lausanne)* 2014;5:224.
47 Simpson A, Petnga W, Macaulay VM, *et al*. Insulin-Like Growth Factor (IGF) Pathway Targeting in Cancer: Role of the IGF Axis and Opportunities for Future Combination Studies. *Target Oncol* 2017;12:571–97.
48 Wang M, Li C, Liu Y, *et al*. Effect of LAMA4 on Prognosis and Its Correlation with Immune Infiltration in Gastric Cancer. *Biomed Res Int* 2021;2021:6428873.
49 Yan J, Wang S-Y, Su Q, *et al*. Targeted immunotherapy rescues pulmonary fibrosis by reducing activated fibroblasts and regulating alveolar cell profile. *Nat Commun* 2025;16:3748.
50 Roberts KJ, Kershner AM, Beachy PA. The Stromal Niche for Epithelial Stem Cells: A Template for Regeneration and a Brake on Malignancy. *Cancer Cell* 2017;32:404–10.